

Article

Supercritical Froude Number Flow through Ducts with Statistically Roughened Walls

Charles R. Ortloff^{1,2}¹ CFD Consultants International, Ltd., 18310 Southview Ave., Los Gatos, CA 95033, USA; ortloff5@aol.com² Research Associate in Anthropology, University of Chicago, Chicago, IL 60637, USA

Abstract: High-speed fluid flows over roughened surfaces occur in many engineering applications; one important application involves high velocity water flows in pipelines with roughened interior walls where the wall roughness affects head loss estimates necessary for engineering design purposes. The present analysis provides an analytical solution of the fluid physics underlying the induced static pressure profile resulting from high Froude number supercritical velocity through duct with random wall roughness. The analytic solution of the hyperbolic governing small perturbation velocity potential equation subject to high Froude number flows brings forward characteristic wave solutions that determine the static pressure profile in a duct with random height wall roughness. While current engineering practice utilizes semi-empirical engineering equations employing test data to determine the friction factor, velocity and static pressure profiles and head loss for different roughness types in different sized ducts as a function of Reynolds number (as summarized in a later section of the paper), the present analysis provides a new analytical method to determine the fluid physics involved in the static pressure change induced by wall random roughness in ducts subject to high Froude number supercritical flows.

Keywords: supercritical flow; Froude number; roughened walls; pressure profile; characteristics



Citation: Ortloff, C.R. Supercritical Froude Number Flow through Ducts with Statistically Roughened Walls. *Water* **2023**, *15*, 2849. <https://doi.org/10.3390/w15152849>

Academic Editor: Vittorio Di Federico

Received: 8 July 2023

Revised: 26 July 2023

Accepted: 1 August 2023

Published: 7 August 2023



Copyright: © 2023 by the author. Licensee MDPI, Basel, Switzerland. This article is an open access article distributed under the terms and conditions of the Creative Commons Attribution (CC BY) license (<https://creativecommons.org/licenses/by/4.0/>).

1. Introduction

Wall roughness on duct walls subject to high speed, high Froude number convective flows has a significant influence on induced pressure and velocity patterns, as well as heat transfer effectiveness. Wall roughness influences and generates perturbations in velocity and as well as static pressure profiles which affect surface drag force, turbulence levels and heat transfer in duct flows. Numerous modern fluid mechanics applications of rough wall flow pattern analysis influencing design and efficiency improvement of mechanical engineering structures, such as turbine flow passageways, turbine blade geometry, piping networks and gas and liquid flows, in machinery systems exist in the literature [1–22]. In addition, applications involving aerodynamic laminar and turbulent boundary layer flow over rough walls [23,24] that influence trajectories and flow resistance changes for aircraft and reentry space vehicles have been studied. Similarly, ocean transport vessels with hull surface roughness operating at high speed experience additional frictional drag effects requiring increased power output affecting their economic efficiency. While surface roughness effects on flows are largely considered to generate negative dissipative energy and increased frictional resistance effects, it has been noted that increased heat transfer also occurs for turbulent flows over roughened walls—this is a positive effect for heat transfer cooling applications of importance to the computer industry where heat production in small, confined device spaces must be controlled to eliminate high temperature excursions. On larger scale applications of flows over roughened surfaces, atmospheric winds flowing around multistory city buildings can be regarded as a situation in which roughness elements influence wind forces on city buildings, that upon analysis, require structural design changes for survivability. On an even larger global scale, mountain ranges

such as the North American Rocky Mountains can be considered as surface roughness that can influence wind and temperature patterns. With the current focus on climate change and global warming effects involving ENSO El Niño and La Niña Pacific Ocean warming, altered wind patterns carrying water vapor have been shown to influence North American coastal hurricane intensities and occurrence frequencies as well as influencing Atlantic Ocean current flows, which in turn affect European countries' climate through land and ocean environments subject to elevated temperatures [21]. Many of these modern-day applications involving small to large scale surface roughness effects on fluid flow patterns can be analyzed from use semi-empirical test equations and CFD analysis. However, high-speed water flows over roughened wall surfaces at different scale sizes continue to present new challenges to understand the fluid physics involved—as demonstrated by copious references addressing problems of this type in the open literature, such as in references [1–20,22–29]. Even in ancient times, the water engineers of the pre-Columbian Peruvian Chimú society (800–1465 CE) recognized that large sidewall roughness elements placed in water transport channels altered flow patterns and eliminated rotation and vortex generation in channel bends, which promoted erosion in unlined channel walls [21]. For this ancient world example, empirical observations made by their water engineers, together with their ingenuity to observe roughness effects on water flow in irrigation channels, provided the continuity to sustain irrigation agriculture over centuries of that society's existence. Further ancient world recognition of wall roughness effects originating from calcium carbonate deposits (sinter) influenced the flow rate in the main channel of the Roman Pont du Gard aqueduct in France. These effects were observed following the deliberate widening of the main channel, done in anticipation of the channel's contraction in time due to sinter deposits [30]. Yet further recognition of wall roughness effects derived from choking sinter deposits were observed at the main Siq pipeline at the Nabataean site of Petra in Jordan (100 BC–300 AD) resulting in the removal of pipeline top halves to convert water flows to open channel type flows—this was recognized by their water engineers as a more efficient way to maintain a vital water flow to the city center [31]. Thus, surface roughness problems influencing water flow patterns have a long history of importance to many different world societies throughout time, that depended upon understanding water flow usage for urban, agricultural and industrial use.

Given the importance of different physical scale applications involving the influence of surface roughness on air and fluid flow patterns in industrial, living standard, climate change and other applications, many investigations [1–20] involving analytical methods have been conducted to understand the fluid physics derived from wall roughness effects of fluid flow patterns. Many investigations involve both laboratory and field experiments to gain an empirical understanding of surface roughness effects on fluid flows. While the reliance on laboratory tests provides usable relevance for many industrial fluid transfer applications, theoretical studies contend with limited theoretical understanding of roughness-induced turbulence evolution and production effects. Furthermore, the accuracy of different theoretical governing equations solutions are challenged to match laboratory test solutions for a wide variety of flow and wall roughness conditions. To address these issues, a theoretical approach leading to a better understanding of the fluid physics involved from wall roughness effects on high Froude number (Fr) fluid flows is needed. A new analysis method is proposed for flows for which inertial flow effects dominate gravitational wave effects; this is noted as $Fr \gg 1$ in the discussion to follow. Such flows can be analyzed by a new theory that emphasizes wave structure creation originating from rough wall structures, that carries pressure and velocity information downstream to influence flow patterns.

The present paper examines two-dimensional fluid flow between roughened duct walls at high supercritical Froude numbers ($Fr \gg 1$). The duct is two dimensional and with random-roughened walls located at $y = \pm a_0/2 + \epsilon N(x)$ from the duct centerline at $y = 0$. The $N(x)$ term represents a wall random roughness function, together with ϵ , the small roughness height factor ($\epsilon \ll 1$) representing the roughness height range on the

upper and lower duct walls. The application considered for analysis represents an initial high-speed supercritical flow entry velocity, U_∞ , at pressure P_0 entering the duct. The object of the analysis is to determine the mean square static pressure distribution induced by the wall roughness. Unlike subcritical Froude number conditions, for which disturbances are spatially damped and upstream influence of wall roughness exists, supercritical flow disturbances emanating from wall roughness exist in the form of Froude waves that originate and propagate downstream from the roughened duct walls. These waves further influence the static pressure and velocity distributions downstream of their roughness origins on duct walls. For supercritical Froude number flows with a free surface, surface waves originating from a disturbance location on the free surface can be observed as forming an acute V-shaped wave structure downstream of the surface disturbance origin point, whose half-angle is given by $\theta = \sin^{-1}(1/Fr)$, as noted in the literature [1–3]. Roughened walls of channels, with flow in the x direction and random roughness patterns with heights in the y direction, influence both the fluid static pressure and velocity distribution throughout the duct interior space.

Of note, references [1–4,6] illustrate the effect of the Froude number on free surface flow patterns over a lower wall obstacle in which the governing equation is $(1 - Fr^2) dy/dx + dz/dx = 0$, where y is the elevated obstacle height and z is the water height over the submerged obstacle in a channel with a free fluid surface. When $Fr > 1$, dz/dx must be positive requiring local surface elevation over the obstacle; when $Fr < 1$, dz/dx must be negative requiring a depressed free surface location above the submerged obstacle. Clearly, the Froude number value (less than or more than unity) has a significantly different influence on the free surface shape and the internal flow pressure and velocity distribution. Unlike subcritical ($Fr < 1$) flows where upstream influence exists to generate downstream disturbances, supercritical $Fr \gg 1$ flow in ducts with upper and lower roughened wall obstacles with an internal flow between the walls produces Froude wave structures that carry static pressure and velocity change information downstream with no upstream influence. The Froude number (Fr) is defined as $Fr = V/(g d)^{1/2}$ where V is the flow velocity, g is the gravitational constant and d is a given effective geometric dimension. For $(Fr)^2$, the numerator is indicative of flow inertial energy while the denominator is indicative of gravitational wave energy. Thus, for a subcritical $Fr < 1$ value in duct flow, gravitational wave energy exceeds the inertial energy-producing upstream influence in the flow from the wall roughness disturbance effects. For supercritical $Fr \gg 1$ duct flows, gravitational wave effects on the flow are much less than flow inertial effects; thus, gravitational effects do not significantly influence the flow and flow inertial effects dominate the flow pattern, with no upstream roughness disturbance effects influencing downstream flows. For the present analysis, supercritical ($Fr \gg 1$) duct flow is characterized by small wall roughness height given by $y = \pm a_0/2 + \epsilon N(x)$ (with $\epsilon \ll 1$), and static pressure disturbances carried by Froude waves originating from wall roughness disturbances are assumed to determine static pressure information. The $N(x)$ stochastic term is characterized by zero autocorrelation in roughness elements, and thus, is termed random roughness. The prediction of the mean square static pressure distribution, $\langle P(1) P(1) \rangle$, follows as a function of the y distance from the duct walls to the duct centerline at $y = 0$, from the analysis to follow, given the flow characteristics described above.

For high-speed gas flows, the use of equations involving Mach number (M) and Mach waves to analyze supersonic gas flow over and within structures is well known. From references [1–3], a similar hyperbolic equation that governs small perturbation effects on fluid flow originating from wall roughness structures governed by wave transmission structures that influence pressure and velocity change can be utilized for water flows. This is done by substituting Fr for M in the linearized governing small perturbation equation that governs static pressure and velocity perturbations, derived from wall roughness origins, and by the use of Froude waves to analyze supercritical water flow in ducts. For Mach number ($M = V/a$) gas flow applications, V is the gas flow speed over (or through) an obstacle and a is the sound speed, that depends upon temperature and air density. For

Froude number ($Fr = V/(g d)^{1/2}$) applications, fluid temperature-dependent flow viscosity and density is present and involves the properties of the working fluid to support wave structure transmission, thus, affecting static pressure and velocity change. For applications involving high-speed ($M \gg 1$) gas flow, the governing equations use Mach number notation; for applications involving high-speed ($Fr \gg 1$) water flows, the governing equation uses Froude number notations, as observed in Equation (1) in the 2.0 analysis section.

For the present analysis, Equation (1) is used with Froude number notation to analyze water flow in a duct with upper and lower duct wall roughness to obtain the mean square pressure distribution induced by the duct wall roughness. As duct wall random roughness elements under $Fr \gg 1$ conditions serve as the disturbances to produce downstream Froude waves carrying downstream static pressure change information, the duct velocity profile is likewise influenced by wall roughness Froude waves. The analysis to follow presents a new method to determine the mean square static pressure distribution, $\langle P(1) P(1) \rangle$ profile, as a function of the y distance from the duct wall to the duct centerline given the fluid mechanics effects of the duct wall's random roughness pattern.

2. Analysis

The small-perturbation equation for supercritical water flow in the roughened walled duct is:

$$\alpha^2 \varphi_{xx} + \varphi_{yy} = 0, \tag{1}$$

where $\alpha = i (Fr_\infty^2 - 1)^{1/2} = i \beta_1$. The quantity φ is the velocity potential, Fr is the free stream Froude number and $i = (-1)^{1/2}$ is the imaginary number designation. From [6], the solution satisfying Equation (1) is:

$$\varphi(x, y) = i\kappa^{(1)} \int_{-\infty}^{\infty} \tilde{N}'(\omega) [\sin(\omega y \beta_1) / \omega \cos(\omega \beta_1 a_0 / 2)] d\omega, \tag{2}$$

where $\kappa^{(1)} = 2/U_\infty \beta_1^{-1}$ and $\tilde{N}'(\omega)$ represents the Fourier transform of the derivative of the wall roughness amplitude function. Following [6,24] (p. 327), the nondimensionalized static pressure distribution, $P(1)$, is given as

$$p^{(1)} / \rho U_\infty^2 \equiv P(1) = -U_\infty^{-1} \varphi_x(1) = P_0^{(1)} (f * g) = P_0^{(1)} \int_{-\infty}^{\infty} g(\omega; y) f(x - \omega) d\omega \tag{3}$$

where ρ is the freestream density, U_∞ the freestream velocity, $p^{(1)}$ is the static pressure, $P_0^{(1)}$ is defined in Equation (3) and the $*$ notation denotes the convolution product.

In Equation (3),

$$f(x - \omega) = N'(x - \omega) \tag{4}$$

In addition,

$$g(x, y) = -2i\mathcal{P} \int_{-\infty}^{\infty} [\sin(\beta_1 \omega y) \cos(\omega x) / \omega \cos(\beta_1 \omega a_0 / 2)] d\omega \tag{5}$$

where \mathcal{P} denotes the principal value. Evaluation of the integral by contour integration [24] for $g(x, y)$ is by means of the RI contour (Figure 1) $x \pm \beta_1 y > 0$ and the contour R11 for $x \pm \beta_1 y < 0$ for x -axis poles $\omega_n = (2n + 1)\pi / \beta_1 a_0$, $n = \pm 1, \pm 2, \pm 3, \dots$ leads to the result:

$$g(x, y) = (i/2) \left\{ \pi + 4 \sum_{n=0}^{\infty} (-1)^{n+1} / (2n + 1) \cdot [(x + \beta_1 y) \cos \pi(2n + 1) / (a_0 \beta_1)] - (x - \beta_1 y) \cos \pi(2n + 1) / (a_0 \beta_1) \right\} H(x \pm \beta_1 y) \tag{6}$$

where $H(t) = 1$ for $t > 0$, $H(t) = -1$ for $t < 0$ and $H(t) = 0$ for $t = 0$. Note that $P^{(1)}$ is real because $\kappa^{(1)}$ and $g(x, y)$ are both imaginary quantities; i.e., the perturbation pressure is a real quantity. From Equation (6), it follows that on the characteristics $x + \beta_1 y$ and $x - \beta_1 y$, the quantity $g(x, y)$ has a constant value, as to be expected, as pressure is constant on a characteristic Froude wave. For a supersonic gas flow, a similar analysis would yield a constant pressure on a characteristic Mach wave. For the present analysis, the Mach-Froude analog can be extended to supercritical perfect fluids, as the current analysis indicates with pressure constant on a Froude wave.

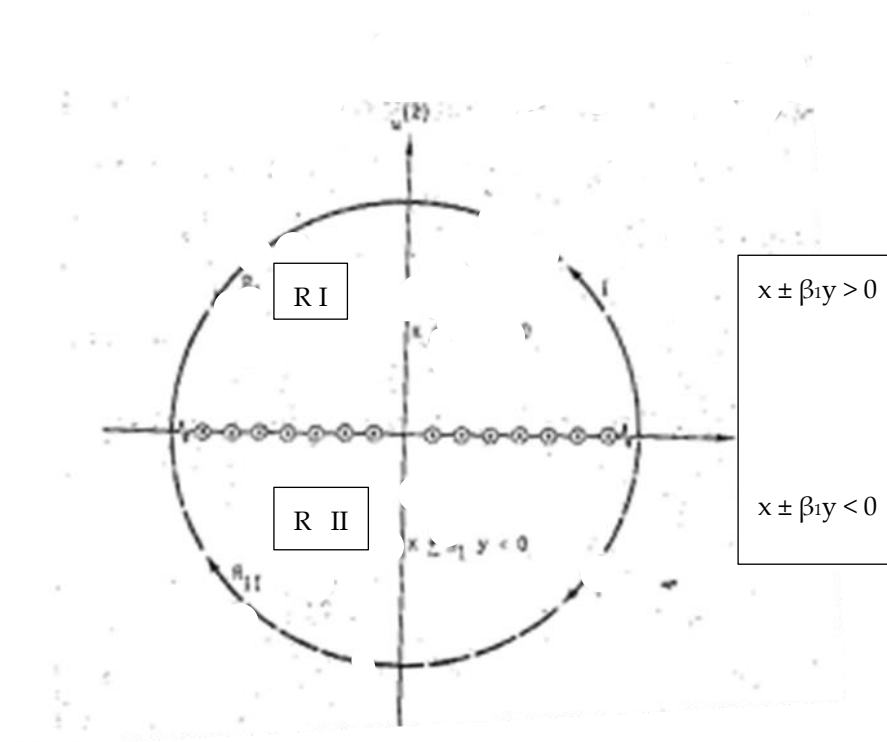


Figure 1. Integration contours for Equation (5) on the ω plane.

In Figure 1, simple poles from Equation (5) continue along the positive and negative x -axis. Note that contour lines R I and R II extend in different directions to accommodate wave structures in regions above and below the duct centerline at $y = 0$. The Equation (5) integral is determined in Equation (6) by the standard $2\pi i$ (sum of the residues) Cauchy integration procedure [24].

The expression of the mean square pressure $\langle P^{(1)} P^{(1)} \rangle$ is given [3] in terms of the stochastic average by:

$$\langle p^{(1)} p^{(1)} \rangle = (P_0^{(1)})^2 \int_{-\infty}^{\infty} \int_{-\infty}^{\infty} g(\xi_1; y) g(\xi_2; y) R_{N'}(\xi_1 - \xi_2) d\xi_1 d\xi_2 \tag{7}$$

where $R_{N'}(\xi_1 - \xi_2)$ is the autocorrelation function of the wall roughness derivative, here taken as the Dirac delta function, to ensure a random roughness wall structure. This case represents the random roughness wall case. Substitution into Equation (5) yields Equation (8):

$$\langle p^{(1)} p^{(1)} \rangle = 32(P_0^{(1)})^2 S_0 \int_{-\infty}^{\infty} \left\{ \sum_{-\infty}^{\infty} (-1)^{n+1} / (2n + 1) \cdot [(\xi_1 + \beta_1 y)^+ \cos\pi(2n + 1) / (a_0 \beta_1) - (\xi_1 + \beta_1 y) - \cos\pi(2n + 1) / (a_0 \beta_1) - (\xi_1 - \beta_1 y)^+ \cdot \cos\pi(2n + 1) / (a_0 \beta_1) + (\xi_1 - \beta_1 y) - \cos\pi(2n + 1) / (a_0 \beta_1)] \right\}^2 d\xi_1 \tag{8}$$

where S_0 is the constant spectral density of the wall roughness derivative distribution. The + and - signs on the $(\xi_1 + \beta_1 y)^+$ and $(\xi_1 - \beta_1 y)^-$ terms denote the two planar characteristics emanating from a point in the two dimensional flow. The physical interpretation of Equation (8) is aided by the following equality:

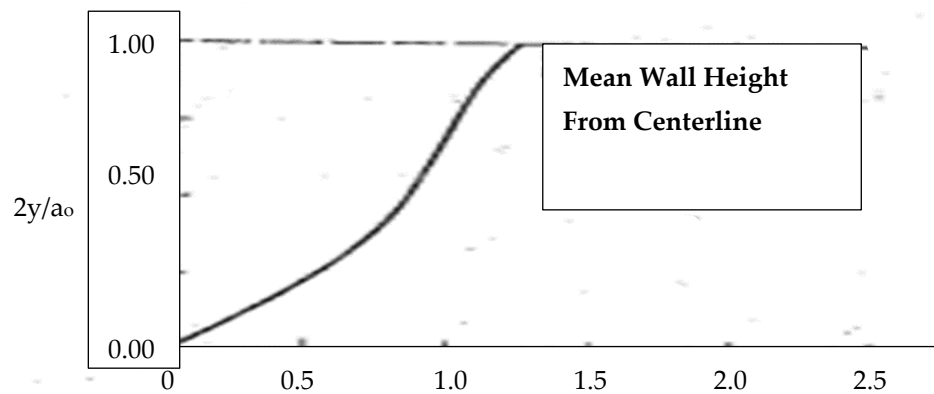
$$\begin{aligned} & -\pi/4, n\pi < x < [(2n + 1)/2]\pi, n = 0, 1, 2, 3, \dots \\ \sum_{n=0}^{\infty} & (-1)^{n+1} / (2n + 1) \cdot \cos x(2n + 1) = 0, x = (2n + 1)\pi/2, n = 0, 1, 2, 3, \dots \quad (9) \\ & +\pi/4, [(2n + 1)/2]\pi < x < (n + 1)\pi, n = 0, 1, 2, 3, \dots \end{aligned}$$

The integrand of Equation (7) represents a periodic structure of Froude waves of slopes $+\beta_1^{-1}$ and $-\beta_1^{-1}$ over $|x| < \infty$, through each of which, a jump of $+\pi/2$ alternates with a jump of $-\pi/2$ after a constant x length behind a Froude number front dictated by Equation (9). The + and - notation on arguments of the cosine functions denotes that arguments greater or less than zero denotes the range of $(\xi \pm \beta_1 y)$. Two classes of Froude waves are represented by Equation (8)—those with slope $-\beta_1$ that originate from the upper duct wall surface $y = a_0/2$, and those with slope $+\beta_1$ that originate from $y = -a_0/2$ wall. These waves originate from the statistically roughened upper and lower walls, respectively. For the supercritical $Fr \gg 1$ case, there is no damping of waves in the y direction (as would exist for the $Fr < 1$ subcritical case); however, the same waveforms are from the upper wall propagated undamped along characteristics of slopes $+\beta_1^{-1}$ from the lower wall and $-\beta_1^{-1}$ from the upper wall. From the linearity of the Equation (1) formulation, there is no interaction between characteristics of slopes $+\beta_1^{-1}$ and $-\beta_1^{-1}$. For flows at critical $Fr = 1$ or $Fr < 1$ subcritical conditions, additional nonlinear terms must be added to Equation (1) that cancel the linearity of the governing equation used for the analysis.

Spatial averaging for the periodic function is next performed over a wavelength. The second and fourth terms which represent the $x < 0$ extension of the periodic function are next dropped, and then subject to Parseval’s theorem, applied to Equation (8) to yield the mean squared pressure distribution shown in Figure 1:

$$\langle p^{(1)} p^{(1)} \rangle = (256/\pi^2) (P_0^{(1)})^2 S_0 \beta_1 \sum_{n=0}^{\infty} (2n + 1)^{-2} [(\sin \pi(2n + 1)/2) \cdot (2y/a_0)]^2 \quad (10)$$

Substitution for $P_0^{(1)}$ in Equation (10) reveals that the mean square pressure varies as the β_1^{-1} angle. As supercritical Froude number increases further toward infinity, the slope of the Froude waves emanating from the roughness disturbances on the duct walls approaches zero. This results in continuance of the nearly undisturbed initial flow in the duct as the domain of influence of the characteristics emanating from wall disturbances contracts to zero area, and therefore the disturbance, $\langle p^{(1)} p^{(1)} \rangle$ is consistent with Equation (10). Essentially, the rough wall disturbances are localized close to the roughened walls for $Fr \gg 1$ flows. The maximum mean square pressure increase occurs on the duct walls for all supercritical Froude numbers as Figure 2 indicates. Unlike for the $Fr < 1$ case, the $Fr \gg 1$ supercritical flow case is characterized by Froude waves emanating from the small wall roughness elements; such waves carry pressure disturbances throughout the duct. Of note [6] is the observation that $\langle P^{(1)} P^{(1)} \rangle$ increases from lower values in the subcritical range as $Fr \rightarrow 1$; from the present case, $\langle P^{(1)} P^{(1)} \rangle$ also increases from lower values in the supercritical range as $Fr \rightarrow 1$. Consequently, the maximum $\langle P^{(1)} P^{(1)} \rangle$ value must necessarily be in the transonic $Fr \approx 1$ range, and therefore requires a nonlinear analysis for accurate transonic flow analysis.



$$\langle P(1) P(1) \rangle \pi^2 \varepsilon^{-2} / 256 \cdot S_0 (P_0^{(1)})^2 \beta_1$$

Figure 2. Mean square static pressure variation vs. normalized duct height.

3. Alternate Empirical Determination of Flow Patterns Originating from Surface Roughness

Among the many ways to analyze fluid flows in roughened wall pipelines and ducts for practical engineering use, wall roughness effects on flows within pipelines have been analyzed by semi-empirical means using experimental data [1] (pp. 56–106) using the relationship $H_f = f (L/D)(V^2/2g)$, where H_f is the head loss, f is a friction factor, L is the pipeline length, V is the flow velocity, g is the gravitational constant and D is an equivalent diameter. Friction factors are available for specific laminar and turbulent flow regimes [1] (p. 105), roughness geometries and heights over a large Reynolds number (Re) range, with f given for rough inner wall pipelines by:

$$F^{-1/2} - 2 \log_{10}(R/\lambda) = 1.75, \tag{11}$$

with R the equivalent pipe radius and λ the longitudinal close spacing of small height roughness elements. The use of empirical Equation (11), together with test data from wide ranges of key parameters, has wide usage in current pipeline system design practice. A further friction factor determinant employing test data is the Fanning friction factor: $f = H_f/(L/D) (V^2/2g)$ which is useful for large Re values for pipeline wall roughness characterized by equivalent sand grain size inner pipeline wall roughness (ε/d) to determine flow head loss H_f for a known input velocity V and Reynolds number. With test-determined graphs involving these parameters [1] (pp. 56–106), the appropriate friction factor can be determined with ε/d , Re and V specified for different laminar and turbulent flow regimes to determine the pipeline head loss H_f . Although flow head loss determination from Equations (11) and (12) have wide use, further equations relying upon semi-empirical methods [7–22,26–29] utilizing log-law structures typical of Equations (11) and (12) are practical and useful for pipeline engineering design work. Little detail of the fluid physics origins that determine the pressure and velocity profiles induced by wall roughness for in sub- and supercritical regimes exists to understand what lies within the test results incorporated in the Equations (11) and (12) empirical approaches, which are only useful for limited range Reynolds number values. Typical of other log-law empirical approaches [29] is Equation (12), originating from von Kármán’s original research in the 1930s. This equation is given by:

$$u/u^* = k^{-1} \ln [(y + h_s/h_L)] + C \tag{12}$$

where u^* = the shear velocity, k is the von Kármán constant (0.4), y is the distance above the wall shear layer, h_s is the wall roughness geometric specification, h_L is the lower wall height and C is a test-related constant. This equation serves in many pipeline head loss studies involving different rough wall types for velocity profile determination and is in use in the present day to support studies involving rough wall effects in fluid flow [8,11–15,18,19,26,27].

The present Section 2 analytical study, therefore, serves to examine and further understand details of the fluid physics underlying the wall roughness effect on the mean square static pressure distribution profile and the velocity profile for supercritical $Fr \gg 1$ flows. This adds to prior analysis [5] done for $M < 1$ subcritical gas flow analysis—as an extension to subcritical Froude number fluid flows, the above analysis can be advanced by replacing $i\beta_1$ by β_1 and the presence of Fr in Equation (1), together with similar analysis methods shown in Section 2. The supercritical flow regime analysis thus far presented in Section 2 provides insight as to how flow head losses originate from wall roughness effects, particularly for high speed ($Fr \gg 1$) supercritical flows where inertial effects far exceed gravity wave effects. The Froude wave analysis analyzed in the above Section 2 determines the static mean square pressure profile, and thus provides detail on the origin of empirical friction factors derived from wall roughness effects for supercritical flows. Turbulent flows involving large viscosity effects for ducts with rough wall structures are termed ‘hyper turbulent flows’, whose analysis to determine the friction factor is given in references [1] (pp. 85–88).

4. Conclusions

The analysis presented examines the effects of small duct wall random roughness variations on a supercritical ($Fr \gg 1$) water flow within the duct to determine the mean square static pressure profile within the duct. The evolved mean square velocity profile can be estimated from the Bernoulli equation

($H_u = V_m^2/2g + p_m/\rho$), where V_m is the mean square velocity distribution, H_u is the total head per unit duct length, ρ is the water density and p_m is the $\langle P^{(1)} P^{(1)} \rangle$ static pressure distribution shown in Figure 2. This is to be applied in the duct area where the wall roughness starts downstream of the unlined smooth wall duct entry area to determine the mean squared velocity profile and head loss, using the mean square static pressure variation induced by the wall roughness. The $\langle P^{(1)} P^{(1)} \rangle$ static pressure is maximal, and the water velocity is minimal at the duct walls, while mean square static pressure is minimal and velocity maximal on the $y = 0$ duct centerline for $Fr \gg 1$ flows. Given that the $Fr \gg 1$ supercritical perturbation flow is governed by Equation (1), analysis results are applicable only for high speed supercritical flow. For cases where Fr is close to a critical unity value ($Fr \approx 1$), additional terms to Equation (1) must be considered as the flow is highly nonlinear. For subcritical ($Fr < 1$) flows where upstream influence from wall roughness exists, additional terms and analysis methods must be employed to determine pressure and velocity profiles.

The near-wall mean square static pressure $\langle P^{(1)} P^{(1)} \rangle$ from Figure 2 achieves a maximum value of the perturbation static pressure on the roughened walls of:

$$\langle P^{(1)} P^{(1)} \rangle = 1.85 (256) \pi^{-2} S_0 (P_0^{(1)})^2 \epsilon^2 \beta_1 \quad (13)$$

and a near zero value toward the duct centerline. This is to be expected, as when $Fr \gg 1$, the β_1 characteristics carrying static pressure information fold closer into the wall, leaving little trace of static pressure perturbation information to affect flows at the duct centerline. As the flow is viscous, the near wall velocity is correspondingly low due to interaction with roughness elements, while the centerline velocity closely retains its input U_∞ value. Thus, for $Fr \gg 1$ supercritical flows in roughened wall ducts, the input flow conditions remain largely undisturbed over most of the duct cross sectional area, given small ϵ values.

As characteristic wave structure proceeds from hyperbolic Equation (1) for $\alpha^2 = (1 - Fr_\infty^2) < 0$ for supercritical $Fr \gg 1$, it can be shown [25] that characteristic angles in the x - y plane emanating from a disturbance are given by:

$$dy/dx = \pm (Fr_\infty^2 - 1)^{1/2}/(1 - Fr_\infty^2), \quad (14)$$

which, for $Fr_\infty \gg 1$, becomes $dy/dx \approx \pm(1/Fr_\infty)$. This is similar in kind to the previously noted $\theta = \sin^{-1}(1/Fr_\infty)$ for observed free surface wave V-shaped structures produced from a surface disturbance. With narrowing β angle wave structures, for $Fr \gg 1$ internal duct fluid flows, pressure and velocity disturbances emanating from the domain of influence associated with wall roughness appear largely confined to the vicinity of small wall roughness elements leading to no or little disturbance of central duct flow regions as Figure 2 indicates. The presence of wave structures as transmitters of pressure and velocity information to the flow from Section 2 analysis, therefore, is consistent with the hyperbolic nature of Equation (1).

A further practical application of the analysis, beyond the Section 1 examples, is that of ship hulls moving at high speeds, with harbor marine hull inclusions characterized as 'roughness elements', which produce additional hull drag that requires higher propulsion energy input to overcome. The present analysis, with large a_0 values, gives details of local static pressure and velocity changes induced by the wall roughness that can be used to determine the additional hull roughness drag additions to add to the smooth hull shape drag coefficient. For submerged ocean objects traveling at high speed, static pressure depends on body shape, and wall roughness effects can alter local surrounding object pressures to limit (or enhance) the occurrence of cavitation vapor bubbles. For military marine environment applications, very high-speed flows over submerged roughened surface vehicles can induce a water vapor envelope environment, through which a vehicle flies under the control of aerodynamic control surfaces. Here, vapor bubble formation proceeds from regions of high stagnation pressures, followed by low pressures that induce vapor bubbles. In this situation, the presence of surface roughness can help to create additional regions of water vapor production to enable the 'flight' of a submerged object moving at high speed. This mixed-flow regime is typical to that created by ship propeller blades rotating at high rotational speeds, that induce vapor bubbles seen in the wake of a passing ship. A further important application of the flow physics associated with surface roughness involves submerged concrete bridge support structures subject to river flows; here wall roughness effects may contribute to erosion of concrete structures through localized surface static pressure fluctuation changes derived from river water velocity fluctuations; this erosion effect is particularly high when river water contains sediments. Further understanding of these and other high Froude number applications are now possible through the use of Section 1 analysis methods.

In summary, there are many practical applications in which flow pressure and velocity changes are induced by a rough wall surface, beyond those described in this and Section 1; many of which, involve roughened walls subject to high $Fr \gg 1$ flows. While semi-empirical test methods are used to evaluate design responses to counter flow-induced problems involving roughened surfaces, the flow physics creating 'body forces' originating from different geometric and surface rough wall conditions is somewhat obscured from test-only laboratory results designed to produce results from scaling laws. To provide aspects of the flow physics producing pressure and velocity profiles originating from rough walls subject to high velocity fluid flow, the Section 2 analysis increases the knowledge on aspects of flow physics involved in relating wall random roughness to induced static pressure and velocity changes affecting the design of a particular structure. For example, an analysis of different types of roughness geometries other than random roughness used in Section 2 may be analyzed by specifying $N(x)$ roughness shapes; this together with Equation (1) provides a method to find a minimum roughness patterns to lower object drag or for heat transfer applications, the optimum roughness pattern to induce a maximum (or minimum) heat transfer coefficient. Given the methodology involved in Section 2, further theoretical studies

may be conducted to understand how different types of roughness can be theoretically analyzed to achieve a desired result, which can later be verified through test results. This, then, is the benefit of the given analysis method.

Funding: This research received no external funding.

Data Availability Statement: Further data available in References.

Conflicts of Interest: The author declares no conflict of interest.

References

- Morris, H.J. *Wiggert Open Channel Hydraulics*; The Ronald Press: New York, NY, USA, 1972.
- Chow, V.T. *Open-Channel Hydraulics*; McGraw-Hill Book Company: New York, NY, USA, 1959.
- Oswatitsch, R. *Gas Dynamics*; Academic Press Inc.: New York, NY, USA, 1986.
- Ortloff, C.R.; Jones, J.P. On the Steady State Flow of a Subsonic Stream through Statistically Roughened Wall Ducts. *J. Acoust. Soc. Am.* **1968**, *44*, 897–902. [[CrossRef](#)]
- Sabersky, R.; Acosta, A.; Hauptmann, E. *Fluid Flow*; The Macmillan Company: New York, NY, USA, 1975.
- Kadivar, M.; Tormey, D.; McGranaghan, D. A review on turbulent flow over rough surfaces: Fundamentals and theories. *Int. J. Thermofluids* **2021**, *10*, 100077. [[CrossRef](#)]
- Onal, U. Correlation of Frictional Drag and Roughness Length Scale for Transitionally and Fully Rough Turbulent Boundary Layers. *Ocean. Eng.* **2015**, *107*, 283–298. [[CrossRef](#)]
- de Marchis, M.; Millici, B.; Napoli, E. Numerical Observations of Turbulence Structure Modifications in Channel Flow over 2-D and 3-D Rough Walls. *Int. J. Heat Fluid Flow* **2015**, *50*, 108–123. [[CrossRef](#)]
- Stimson, M.; Snyder, J.; Thule, K.; Mangillo, D. Scaling Roughness Effects on Pressure Loss and Heat Transfer of Additively Manufactured Channels. *J. Turbomach.* **2017**, *139*, 021003. [[CrossRef](#)]
- Piomelli, U. Recent Advances in Numerical Simulation of Rough Wall Boundary Layers. *Phys. Chem.* **2019**, *25*, 63–72. [[CrossRef](#)]
- Volino, R.; Schulz, M.; Flack, K. Turbulence Structure in a Boundary Layer with 2-D Roughness. *J. Fluid Mech.* **2009**, *665*, 75–101. [[CrossRef](#)]
- Allen, J.; Shockling, M.; Kunfel, G.; Smith, A. Turbulent Flow over Smooth and Rough Surfaces. *Philos. Trans. R. Soc. Math. Phys. Sci.* **2007**, *365*, 699–714.
- Grass, A. Structural Features of Turbulent Flow over Smooth and Rough Boundaries. *J. Fluid Mech.* **1971**, *30*, 233–255. [[CrossRef](#)]
- Taylor, J.; Carrano, A.; Kandlikar, S. Characterization of the Effects of Surface Roughness and Texture on Fluid Flow- Past, Present and Future. *Int. J. Therm. Sci.* **2006**, *45*, 962–968. [[CrossRef](#)]
- Schneider, S. Effects of Roughness on Hypersonic Boundary Layer Transition. *J. Spacecr. Rocket.* **2006**, *45*, 193–208. [[CrossRef](#)]
- Wei, L.; Ge, X.; George, J.; Durbin, P. *Modeling Transition on Smooth and Rough Blades*, American Society of Mechanical Engineering, Fluids Division; ASME Transactions: New York, NY, USA, 2016.
- Robert, S.; Yaras, M. Boundary Layer Transition Affected by Surface Roughness and Free Stream Turbulence. *J. Fluid Eng. ASME Trans.* **2005**, *127*, 449–457. [[CrossRef](#)]
- Muppidi, K.; Mahesh, K. Direct Numerical Simulation of Roughness-Induced Transition in Supersonic Boundary Layers. *J. Fluid Mech.* **2012**, *693*, 28–56. [[CrossRef](#)]
- Boyle, R.; Sonyitko, R. Measurements and Predictions of Surface Roughness on Turbulent Boundary Layer Aerodynamics. *ASME Gas Turbine Inst. EXPO Publ.* **2003**, *36894*, 291–303.
- Dryden, H. Review of Published Data on the Effect of Roughness on Transition from Laminar to Turbulent Flow. *J. Aerospace* **1952**, *20*, 477–482. [[CrossRef](#)]
- Ortloff, C.R. *Water Engineering in the Ancient World: Archaeological and Climate Perspectives on Societies of Ancient South America, the Middle East and South-East Asia*; Oxford University Press: Oxford, UK, 2010.
- Ortloff, C.R. Wall Roughness Effects on Inviscid Nonequilibrium Flow in Ducts, Aerospace. Corporation Report-269(4230-20)-6, (U), 1964.
- Ortloff, C.R. Hypersonic Near Free Molecule Flow over a Sharp Leading Edge Flat Plate with a Small Thermal Accommodation Coefficient. *Astronaut. Acta* **1970**, *15*, 215–229.
- Carrier, G.; Krook, M. *Functions of a Complex Variable: Theory and Technique*; McGraw-Hill Book Company: New York, NY, USA, 1966; p. 327.
- Bitsadze, A. *Equations of the Mixed Type*; The Macmillan Company: New York, NY, USA, 1966; pp. 1–5.
- von Kármán, T. *Mechanical Similitude and Turbulence*; NACA Technical Memo No. 611; NACA: Boston, MA, USA, 1930; Volume 7.
- Smart, G. A Base for the Log Law and von Kármán's Constant Problem. *J. Hydraul. Res.* **2022**, *60*, 935–943. [[CrossRef](#)]
- Cheng, N. Formulas for Friction Factors in Transitional Regimes. *Hydraul. Eng.* **2008**, *134*, 1357–1362. [[CrossRef](#)]

29. Mofrad, M.; Afzalimehr, H.; Parvizi, P.; Ahmad, S. Comparison of Velocity and Reynolds Stress Distributions in a Straight Rectangular Channel with Submerged and Emergent Vegetation. *Water* **2023**, *15*, 2435. [[CrossRef](#)]
30. Ortloff, C.R. *The Hydraulic State: Science and Society in the Ancient World*; Routledge Publishers: London, UK, 2021; pp. 295–318.
31. Ortloff, C.R. Hydraulic Engineering at 100 BC- 300 AD Nabataean Petra (Jordan). *Water* **2022**, *12*, 3498. [[CrossRef](#)]

Disclaimer/Publisher’s Note: The statements, opinions and data contained in all publications are solely those of the individual author(s) and contributor(s) and not of MDPI and/or the editor(s). MDPI and/or the editor(s) disclaim responsibility for any injury to people or property resulting from any ideas, methods, instructions or products referred to in the content.